International Journal of Heat and Mass Transfer 139 (2019) 1077–1086

Contents lists available at ScienceDirect

International Journal of Heat and Mass Transfer

journal homepage: www.elsevier.com/locate/ijhmt

Cyclic characteristics of water thermocline storage tank with encapsulated PCM packed bed

Zhaoyu He [a], Xiaohui Wang [a], Xiaoze Du [b,a,*], Chao Xu [a], Lijun Yang [a]

[a] Key Laboratory of Condition Monitoring and Control for Power Plant Equipment (North China Electric Power University), Ministry of Education, Beijing 102206, China
[b] School of Energy and Power Engineering, Lanzhou University of Technology, Lanzhou 730050, China

ARTICLE INFO

Article history:
Received 16 February 2019
Received in revised form 18 May 2019
Accepted 27 May 2019
Available online 3 June 2019

Keywords:
Thermal energy storage (TES)
Thermocline
Phase change material (PCM)
Packed bed
Cyclic characteristic

ABSTRACT

Thermal energy storage (TES) with phase change materials is a promising approach for combined heat and power plants to enhance the electricity peak regulation capability and maintain stable heat-supply at the same time. Its cyclic performance is important under practical working conditions, however was rarely investigated. An experimental study on the thermocline TES was presented employing encapsulated paraffin wax packed bed as heat storage media and water as heat transfer fluid (HTF). The cyclic characteristics were revealed experimentally with consecutive charging/discharging processes. Convergence behavior was observed during the cyclic operation. It was found that the end-of-charging/discharging temperature distribution, charging/discharging duration and utilization rate of each cycle tend to be stable as the cycle number increases. It is believed that such behavior stems from the difference between the initial status and the end-of-charging/discharging criteria. The influences of flow rate of HTF, working temperature and initial status on the operational performance were investigated. The results indicated that the initial status had no significant impact on the TES performance after the convergence reached. Larger flow rate of HTF resulted in lower utilization rate and longer duration of each cycle. Especially the cyclic operation performance was strongly depended on the completeness of charging/discharging. These results may be helpful to understand such promising thermal energy storage technology, as well as the design and improvement of its auxiliary system.

1. Introduction

To alleviate the crisis of global warming and air pollution, more and more renewable energy power generation, instead of that of fossil fuel, such as solar power and wind power, has been put into operation in recent years. To maximize the advantage of renewable energy, most combined heat and power (CHP) plants using fossil fuels should be responsible for the electricity peak regulation. However, as the electricity demand usually reaches the peak in the daytime while the heat-supply demand in the midnight, the mismatch between electricity and heat-supply demand leads to a major operational problem, i.e. the compromise of the power regulation capability if the stability of heat-supply is taken as priority. To make up the mismatch problem and lower the operation cost, thermal energy storage (TES) plays an important role in the energy deployment of power generation and heat-supply in the CHP plants [1,2]. With TES systems, the electricity generation can be adjusted according to the actual demand during the heating period. In the meantime, the abundant heat is stored temporarily and then released to the heat-supply network.

Till now, most TES systems for CHP plants are single-tank or two-tank TES system. Compared to the two-tank TES, where the cold and hot working fluids are stored in two tanks separately, single-tank TES usually occupies less land and costs less initial investment [3]. Based on the density difference between the cold and hot fluids, the cold and hot region is separated along the vertical direction inside the tank and such phenomena can be maintained by the buoyancy force for a long time. The area between the cold and hot region where there exists substantial temperature gradient is defined as the thermocline. During the charging process, hot fluid enters the tank from the top. The hot region becomes larger and the thermocline moves downward. On the contrary, during the discharging, cold fluid enters from the bottom and the thermocline gradually moves upward. In this way, thermal energy can be stored by the working fluid in the form of sensible heat. Generally, smaller thermocline thickness implies better stratification performance, which results in higher efficiency of thermal energy utilization. It has been reported from both numerical and

* Corresponding author at: School of Energy and Power Engineering, Lanzhou University of Technology, Lanzhou 730050, China.
E-mail address: duxz@ncepu.edu.cn (X. Du).

https://doi.org/10.1016/j.ijheatmasstransfer.2019.05.093
0017-9310/

Nomenclatures

c	specific heat (kJ/(kg·K))
E	energy (MJ)
Δh	fusion heat (kJ/kg)
Q_v	volume flow rate (m^3/h)
T	temperature (°C)
V	volume (m^3)
ε	porosity (–)
λ	thermal conductivity (W/(m·K))
ρ	density (kg/m^3)

Subscripts

C	charging
D	discharging
in	inlet
l	liquid phase
out	outlet
p	paraffin wax
s	solid phase
ss	stainless steel shell of PCM capsules
w	water

Superscripts

*	dimensionless diameter

Abbreviations

CHP	combined heat and power
CSP	concentrated solar power
PCM	phase change material
PCT	phase change temperature
ST	switching temperature
TES	thermal energy storage
UR	utilization rate

experimental study that the thermocline expands gradually and its thickness is strongly related to the charging/discharging flow rate. Stratification of fluid-based TES can be destroyed by plume entrainment, inlet jet mixing, thermal conduction and diffusion within the working fluid in the tank [4].

At present, molten salt, thermal oil and water are the main storage medium used in utility-scale TES system. Among them, molten salt and thermal oil are suitable for high-temperature TES, such as the concentrated solar power (CSP), because of their great balance of capacity, cost, efficiency and usability at high temperatures [5]. As for the medium- and low-temperature TES in CHP plants, water is more appropriate because of its great availability and it can be used for heat-supply directly. Although single-tank heat storage technologies are well developed and have already been applied in some CSP and CHP plants, their energy storage density is limited compared to the latent heat energy storage. To improve this issue, it is effective to arrange phase change material (PCM) inside the tank. In order to avoid leakage and overcome the disadvantage of low thermal conductivity of most PCM, the PCM has to be contained in other materials with high thermal conductivity, such as stainless steel and aluminum. Most pilot-scale experimental studies employed PCM modules or PCM capsules with the formation of packed bed TES tank.

Previous investigations on packed bed thermocline storage tank are mainly for high-temperature TES, in which sands or rocks are used as filter to reduce the usage of thermal oil, which is expensive. In contrast, for water tank, because the cost for both building and operation is relatively low, it is possible to select a suitable PCM to enlarge its heat storage capacity, pursuing better economic and social benefits. In the past decade, numerous researches have been conducted on the PCM packed bed tank, focusing on the overall thermal or hydrodynamic performance [6–11], the heat transfer difference among PCM capsules of different positions within the packed bed region [12,13] and within a certain PCM capsule [11,13,14] as well. It has been proved both experimentally and numerically that the employment of PCM packed bed has a significant influence on a series of performance, including that of temperature distribution, stratification behavior, charging time, energy efficiency, MIX number and Richardson number [6,7,15]. Meanwhile, methods have been developed to enhance the accuracy for encapsulated PCM packed bed simulation [16], correlations calculating the phase change process within the capsule [17], and improve the performance of PCM packed bed storage tank, such as using smaller PCM particles, multiple-type PCM packed bed and multiple granular phase change components [8,18–20].

These results benefit a lot the understanding of the PCM packed bed thermocline heat storage. However, the single-tank TES usually operates with repetitive charging/discharging cycles. The cyclic performance of water thermocline storage tank with PCM packed bed is a rather neglected area to be studied, especially by experiments. Nithyanandam et al. [21,22] proposed a methodology for the design and optimization of encapsulated PCM TES system for CSP plant operating conditions based on repeated charging and discharging cycles. By numerical simulation, Wu et al. [18] have compared the cyclic behaviors of the molten salt packed bed TES with non-cascaded PCM packed bed and cascaded packed bed with three and five phase change temperatures (PCTs) ranging from 305 °C to 375 °C. They concluded that the cascaded system had faster discharging and charging rate and the repeatable state could be reached after some cycles. Most previous investigations on the cyclic operation of packed bed TES tank devoted to the application of high-temperature TES, employing oil, molten salt or air as HTF and rocks rather than PCM as packed bed. Bruch et al. [23,24] carried out experimental investigations on the cycling behavior of the thermal oil storage system filling with a mixture of silica gravel and silica sand as packed bed. Li et al. [25] conducted the cyclic analysis of a multi-layer packed bed molten salt thermocline tank using high-temperature concrete, silicon carbide, alumina ceramics, cast iron and quartzite rock as solid filter. Employing pebbles as packed bed and air as HTF, McTigue et al. [26] have numerically studied the performance response of the packed bed thermal storage to repeated charge-discharge cycles and cycle duration perturbations. Although these researches have concentrated on various packed bed TES systems with different HTF and materials for the packed bed filter, all of them indicate that there exists a great difference between the cyclic operation behaviors and the single charging or discharging process. Therefore, the cyclic investigations are of great values for both research and applications.

As the expansion of the authors' prior work [27], in which the thermal performance of water thermocline storage with encapsulated PCM packed bed was discussed, the aim of the present study is to further investigate its characteristics when repetitive charging and discharging are involved. Aiming at the background of thermal storage for enhancing the electric power regulation capability of

CHP plants and domestic heat-supply, water continues to serve as HTF and paraffin wax as filter of capsules to build the PCM packed bed. The general pattern of the water thermocline storage tank with PCM packed bed under cyclic operation will be presented, along with the analysis on the influence of various operational parameters/conditions such as initial status, flow rate, working temperature range and the criteria for the end of charging/discharging.

2. Experimentation

2.1. Experimental system

Composed by the charging and discharging loop, the experimental system is illustrated in Fig. 1. As shown in Fig. 1(a), the saturated steam produced by the steam generator serves as the heat source of charging while the chilling water is the cold source for discharging. The main body of the TES tank is of 0.9 m in inner diameter and 1.1 m in height. The whole volume is about 0.75 m^3 along with the conical bottom. An orifice plate is fixed at the bottom of the TES tank to support the paraffin wax capsules, which are piled up randomly till the top of the tank to build the encapsulated PCM packed bed.

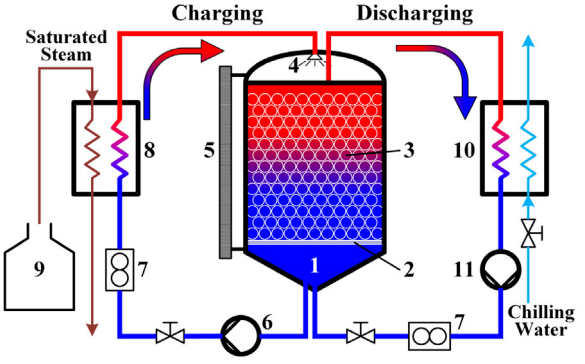

1-TES tank; 2-Orifice plate; 3-Paraffin wax capsules; 4-Spiral nozzle; 5-Liquid level gauge; 6-Pump A; 7-Flow meter; 8-Plate heat exchanger A; 9-Steam generator; 10-Plate heat exchanger B; 11-Pump B

(a) Flowchart of the experiments.

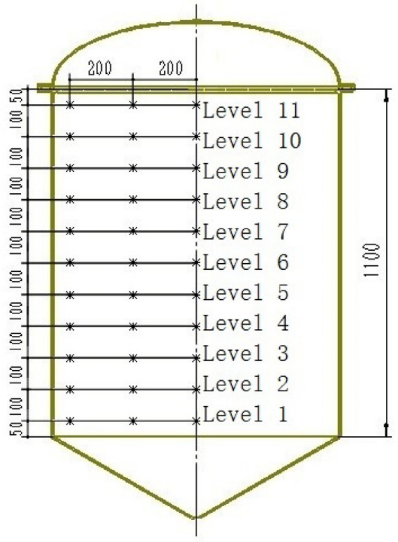

(b) Thermocouples distribution within the tank, in mm.

Fig. 1. Schematic of the experimental setup [27]. (a) Flowchart of the experiments. (b) Thermocouples distribution within the tank, in mm.

K-type thermocouples with the precision of ±0.5 °C are employed to measure the temperature field within the TES tank and some pivotal positions outside the tank as well. The thermocouples inside the tank are divided into 11 groups, fixed at different height with equal distance, which are shown in Fig. 1(b). Other temperature measuring points are responsible for monitoring the inlet and outlet HTF temperature of charging/discharging loop and the ambient temperature. All of the temperature data are recorded automatically by the data acquisition instrument every 10 s. To minimize the heat dissipation, the whole TES tank is equipped with 35 mm foam rubber as thermal insulation, whose thermal conductivity is 0.034 W/(m·K).

The detail of the experimental setup can also refer to literature [27].

In the present study, water serves as the HTF and secondary TES media, while encapsulated paraffin wax capsules are the primary TES media. The thin shell of PCM capsules is made of stainless steel. Sharma et al. [28] reported that paraffin wax consists of a mixture of mostly straight chain *n*-alkanes, whose physical properties including the melting point and latent heat are relevant to the chain length (the number of carbon atoms). Technical grade hentriacontane (CH_3-$(CH_2)_{29}$-CH_3), one kind of paraffin wax, is used as PCM. As small amount of impurity is involved, the PCT, latent heat of fusion and specific heat of the PCM are obtained with the differential scanning calorimetry (DSC) test. The thermo-physical properties of the adopted paraffin wax and technical parameters of PCM capsules are presented in Table 1. Totally 9170 PCM capsules are arranged inside the tank to build the PCM packed bed.

The porosity of PCM packed bed can be obtained by,

$$\varepsilon = 1 - \frac{9170 V_{capsule}}{V_{packed-bed}} \tag{1}$$

where ε is the porosity, $V_{capsule}$ and $V_{packed\text{-}bed}$ are the volume of a capsule and the whole volume of packed bed area including the void, respectively.

The porosity of PCM packed bed is 0.379.

The theoretical heat storage capacity of the TES tank can be acquired by,

$$E_{total} = E_w + E_p + E_{ss} \tag{2}$$

where E_w, E_p, and E_{ss} are the thermal energy stored by water, paraffin wax and stainless steel shell, respectively. They can be attained as follows,

$$E_w = M_w c_w (T_{ini} - T_{in}) \tag{3}$$

Table 1
Thermo-physical properties of paraffin wax and technical parameters of PCM capsules.

Paraffin wax	Value
Solid-liquid phase change temperature range, T_{pc}	67–69 °C
Fusion heat, Δh	254 kJ/kg
Specific heat (solid phase), $c_{p,s}$	2.15 kJ/(kg·K)
Specific heat (liquid phase), $c_{p,l}$	2.19 kJ/(kg·K)
Density (solid phase), $\rho_{p,s}$	0.838 kg/m^3
Density (liquid phase), $\rho_{p,l}$	0.834 kg/m^3
Thermal conductivity (solid phase), $\lambda_{p,s}$	0.21 W/(m·K) [29]
PCM capsules	**Value**
Inner diameter	41 mm
Outer diameter	42 mm
Filling fraction	80%
Mass of paraffin wax	25 g
Specific heat of the shell (at 20 °C), c_{ss}	0.5 kJ/(kg·K)
Density of the shell (at 20 °C), ρ_{ss}	7930 kg/m^3

$$E_p = M_p\left[c_{p,s}(67\ ^\circ\mathrm{C} - T_{in}) + \Delta h + c_{p,l}(T_{ini} - 69\ ^\circ\mathrm{C})\right] \quad (4)$$

$$E_{ss} = M_{ss}c_{ss}(T_{ini} - T_{in}) \quad (5)$$

With Eqs. (2)–(5), the energy storage capacity is calculated as the thermal energy difference between the totally discharged status and the totally charged status. Therefore, the value of thermophysical properties should take the mean of the both statuses for calculation. It is obtained that the theoretical heat storage capacity of the present TES tank is 130.37 MJ with the temperature varies from 50 °C to 83 °C. Its energy storage density is enhanced by 29.62% compared to that of the conventional pure water storage tank calculated under the same boundary conditions. The comparison is shown in Fig. 2. In addition, it should be noted that water stored within the conical bottom of the tank is also included in the calculation for both tanks.

To better compare the performance of different working conditions, the charging/discharging utilization rate, UR, can be calculated according to Eq. (6). Based on the first law of thermodynamics, UR is the ratio of the actual amount of heat stored/released in each charging/discharging to the theoretical heat storage capacity of the TES tank.

$$UR = \frac{\int_0^{\tau_{end}} |T_{in}(\tau) - T_{out}(\tau)| c_{p,w} Q_v \rho_w \mathrm{d}\tau}{E_{total}} \quad (6)$$

Note that the temperature data are recorded every 10 s during the experiments, the functions of $T_{in}(\tau)$ and $T_{out}(\tau)$ are not continuous. Hence, Eq. (6) has to be modified as,

$$UR = \frac{\sum_{i=1}^{i=n-1} |T_{in,i} - T_{out,i}| c_{p,w} Q_v \rho_w \Delta\tau}{E_{total}} \quad (7)$$

2.2. Experimental procedure

For most cyclic operations investigated, initially the TES tank is considered totally discharged as all of the 33 temperature measuring points within the tank have the temperature difference of $T_D \pm 1.0$ °C. As the influence of initial condition is also studied, cases in which the TES tank with initial status of totally charged, i.e., all the thermocouples within the tank shows temperature difference of $T_C \pm 1.0$ °C, are presented in the following Section 3.2. Measured by the liquid level gauge, water level maintains at the joint of the cylindrical main body and the dome top of the tank, as shown in Fig. 1(a), during each experiment.

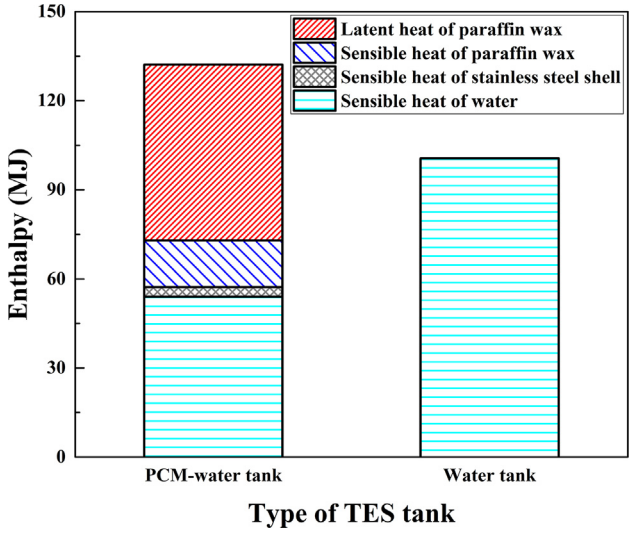

Fig. 2. Energy storage comparison of PCM-water tank and conventional water tank (50–83 °C).

During the operations, charging and discharging processes follow one after another without any pauses or standby periods. The substitution of charging and discharging is determined by the outlet HTF temperature, T_{out}, i.e., the cold outlet water temperature during the charging and the hot outlet water temperature during the discharging. Switching temperatures are defined as the criteria to decide when the charging or discharging stops and then turns into the next discharging or charging. For the charging process, $T_{out,C}$ gradually climbs up. Once it reaches the charging switching temperature, the charging is stopped and the discharging starts. On the contrary, $T_{out,D}$ gradually comes down during the discharging and the moment T_{out} falls below the discharging switching temperature, the discharging is replaced by the charging.

Referring to [23], dimensionless charging and discharging switching temperature are defined as,

$$ST_C^* = \frac{ST_C - T_{D,in}}{T_{C,in} - T_{D,in}} \quad (8)$$

$$ST_D^* = \frac{T_{C,in} - ST_D}{T_{C,in} - T_{D,in}} \quad (9)$$

These parameters range from 0 to 1. Higher value indicates that the charging/discharging is more complete. For example, ST_C^* close to 1 corresponds to the charging process ending with almost fully charged status.

Despite the substitutions of charging and discharging, the charging/discharging flow rates, Q_v, and inlet HTF temperatures, T_{in}, of each cycle are maintained stable at the predetermined value during the entire cyclic operation.

3. Results with analysis

3.1. General behavior

Drafted with linear interpolation according to the collected experimental data, a series of 2D temperature distributions within the TES tank when each charging/discharging completes during the cyclic operation starting from totally discharged is shown in Fig. 3. "Cn" and "Dn" refer to the nth charging and discharging, respectively. The isotherms of 67.0 °C and 69.0 °C, which are the lower and upper limits of the PCT range of the paraffin wax, are also presented.

It can be found from Fig. 3 that significant difference emerges in the first nine cycles, i.e., the left four pairs of temperature fields. After the 9th cycle, the temperature distributions become almost the same. For the charging, hot region expands since C1 and becomes stable after C9. As the cycle number increases, both two presented isotherms move downward, but that of 69.0 °C has more remarkable movement than that of 67.0 °C. For the discharging, it exhibits the opposite behavior to the charging. Cold region expands before D9 and reaches stable after that. The isotherm of 67.0 °C shows distinct movement while that of 69.0 °C remains at almost the same axial position since D1.

In addition, as Fig. 3 shows, the radial temperature difference is not obvious, indicating that the thermal insulation has been well equipped and the water distributor is appropriate for this experimental study. In this case, the temperature distribution can be simplified to the one-dimensional distribution. Hence, in the later discussion, the temperatures of each axial position are obtained by the mean value of the three temperatures detected at the same axial position as shown in Fig. 1(b).

The temperature distribution curves are shown in Fig. 4(a), which reflects similar pattern of temperature evolution as Fig. 3

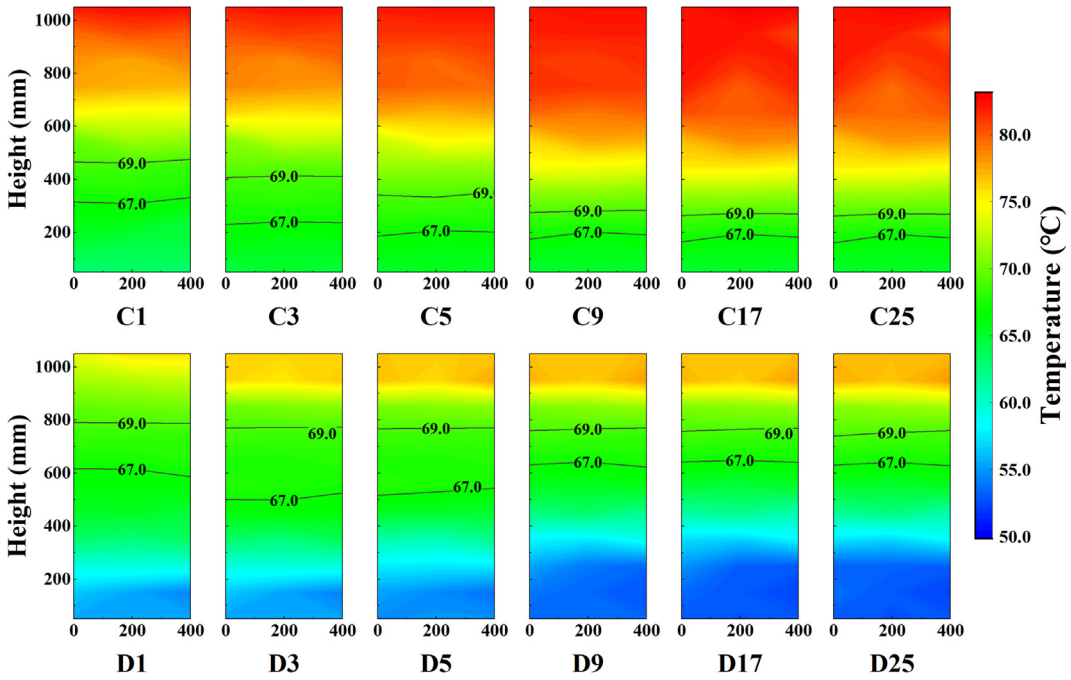

Fig. 3. 2D temperature distributions of the ends of each charging and discharging (T_C = 83 °C, T_D = 50 °C, ST_C = 57 °C, ST_D = 78 °C, Q_v = 0.90 m^3/h).

does. The temperature curves tend to be steeper as the cycle number increases. The curves of charging and discharging come to be convergent separately. Such convergence behavior is more apparent in the upper region, where the temperature is higher than the PCT, for the charging while in the bottom region, where the temperature is lower than the PCT, for the discharging.

Fig. 4(b) shows the variations of UR and duration of each charging and discharging. It can be seen that both UR and charging/discharging duration demonstrate convergence like the evolution of temperature distribution. They gradually increase at the growth rate decreasing with cycle number. After the 9th cycle, the charging and discharging UR are stable at around 17.7% and 17.5%, respectively. The charging and discharging duration are stable at around 12.7 min and 12.1 min, respectively.

Compared to other charging processes, it is obvious that much higher UR and longer duration appear in C1. This may be caused by the specialty of the initial status. Shown as D0 in Fig. 4(a), C1 begins with the totally discharged status, which is much different from the initial status of other charging processes. It needs more time to reach the terminate condition, i.e., the HTF outlet temperature reaches 57.0 °C. Hence, more thermal energy is stored inside the TES tank in C1, leading to higher charging UR and longer charging duration. More detailed discussion on this behavior will be presented later in Section 3.4. As the terminate condition of charging/discharging remains unchanged, the temperature distribution of the ends of charging/discharging come to be identical separately, resulting in the convergence of UR and duration of charging/discharging.

Additionally, the thermal energy difference between that stored during C1 and that released during D1 consists of two parts: heat dissipated to the environment and energy remaining within the tank. As the released energy during discharging is always less than the energy stored during charging in each cycle, it seems that the second part will never leave the tank from the discharging outlet during all of the following discharging processes, becoming kind of "inherent energy" within the TES tank.

3.2. Influence of initial condition

Fig. 5 presents the comparison of two cyclic operations with different initial status. One starts from totally discharged, shown as D0 in Fig. 5(a), and another starts from totally charged, shown as C0 in Fig. 5(a). Profiles with solid symbols represent the cyclic operation starting with totally discharged, while hollow symbols represent the initial status of fully charged. It can be seen from Fig. 5(a) that the cyclic operation starting with totally charged spends less cycles to reach the stability of temperature distribution. For the both cases, the temperature profiles are highly coincident after the convergence is completed.

Similar trend is also observed in the evolution of charging/discharging duration and UR as shown in Fig. 5(b) and (c), respectively. The charging/discharging duration and UR are considered convergent when their change rates are less than 5%. Both the duration of single charging/discharging and UR are close to each other after the 9th cycle for the both cases, which means that the initial status for cyclic operation makes no difference to the charging/discharging duration and UR after convergence.

However, it takes more cycles to converge when it begins with totally discharged. Consequently, conclusions can be drawn that the initial condition has little effect on the temperature distribution, charging/discharging UR and duration when the convergence is completed. On the other hand, the convergence speed is greatly influenced by the initial status. Cyclic operation starting with totally charged reach the convergence faster than starting with totally discharged. This phenomenon may be related to the difference of water distributor of the inlet of charging and discharging. The specific reason still needs to be further studied.

3.3. Influence of flow rate and temperature range

As listed in Table 2, the convergent temperature distribution, charging/discharging UR and duration of the cyclic operation with different volume flow rates, 0.50 m^3/h and 0.90 m^3/h, and working

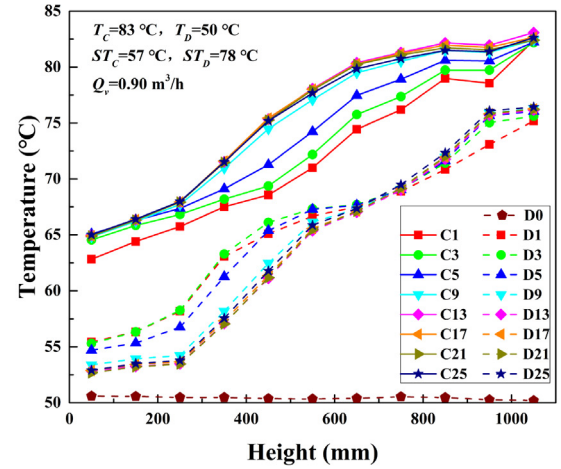

(a) Temperature profiles of the ends of each charging/discharging.

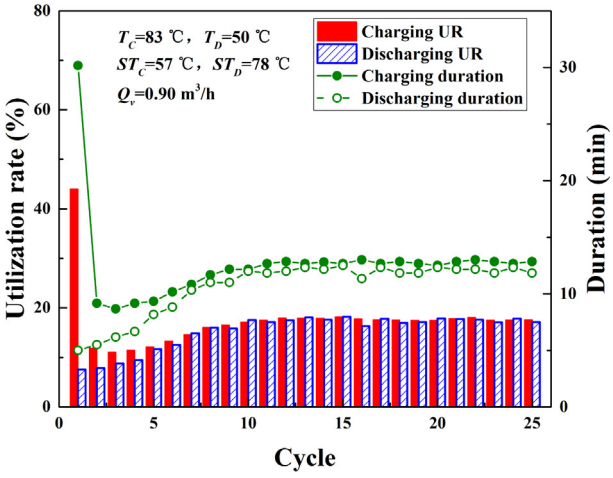

(b) Variations of utilization rate and duration of each charging/discharging.

Fig. 4. General behavior of cyclic operation. (a) Temperature profiles of the ends of each charging/discharging; (b) Variations of utilization rate and duration of each charging/discharging.

temperatures, T_C = 73 °C, T_D = 40 °C and T_C = 83 °C, T_D = 50 °C, are illustrated in Fig. 6. It should be noted that Fig. 6(a) showed the temperature profiles of the end of the last charging/discharging of each case, representing the convergent temperature distribution.

As expected, the charging/discharging duration is much shorter under large flow rate. Presented in Fig. 6(b), operation under flow rate of 0.90 m³/h spends less than half the time to complete a single charging/discharging than operation under flow rate of 0.50 m³/h. When T_C = 83 °C, T_D = 50 °C, the charging and discharging durations at flow rate of 0.50 m³/h are 26.0 min and 24.0 min, respectively, while it drops to 12.7 min and 12.1 min respectively at flow rate 0.90 m³/h. As for the working condition that T_C = 73 °C, T_D = 40 °C, the charging and discharging durations decline from 27.2 min to 13.6 min and from 25.8 min to 12.9 min, respectively, if the flow rate increases from 0.50 m³/h to 0.90 m³/h. Besides, difference of convergent temperature distribution between the two investigated flow rates is obscure as

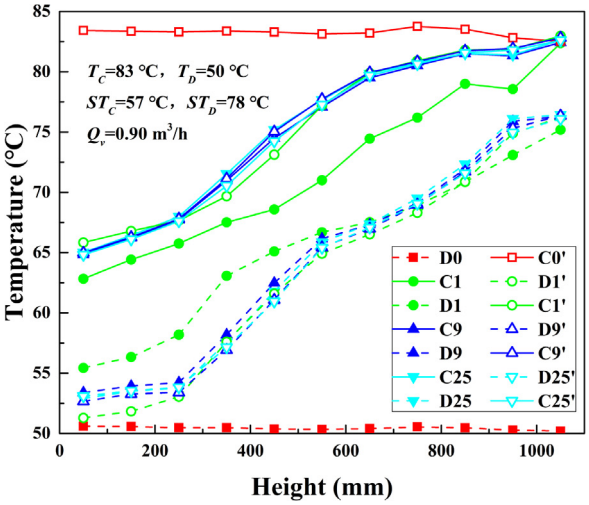

(a) Temperature distribution profiles of the ends of each charging/discharging.

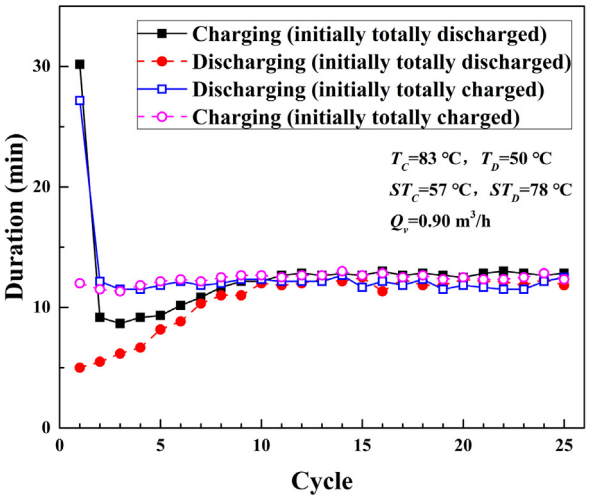

(b) Charging and discharging duration.

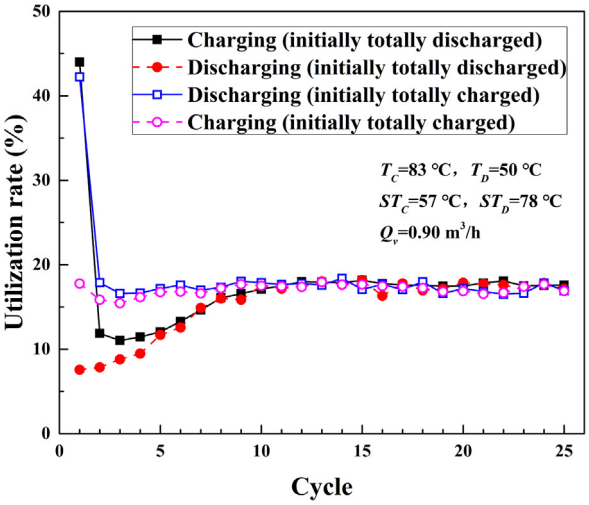

(c) Charging and discharging utilization rate.

Fig. 5. Comparison of cyclic operation with different initial status. (a) Temperature distribution profiles of the ends of each charging/discharging; (b) Charging and discharging duration; (c) Charging and discharging utilization rate.

Table 2
Working conditions for the experiments with different flow rates and working temperatures.

Case	Q_v (m^3/h)	T_D/T_C (°C)	ST_C/ST_D (°C)	(ST_C^*, ST_D^*)
3-1	0.50	40/73	47/68	(0.21, 0.15)
3-2	0.90	40/73	47/68	(0.21, 0.15)
3-3	0.50	50/83	57/78	(0.21, 0.15)
3-4	0.90	50/83	57/78	(0.21, 0.15)

shown in Fig. 6(a). However, from the prospective of charging/discharging UR as shown in Fig. 6(c), large flow rate leads to lower UR, which is like the performance of single charging/discharging.

Compared with the flow rate of 0.50 m^3/h, the charging and discharging UR are closer under the flow rate of 0.90 m^3/h. Thus higher thermal efficiency can be obtained by increasing the working flow rate to shorten the charging/discharging duration, leading to less heat dissipation during each cycle.

As for the influence of working temperature range, on the one hand, it does not show obvious correlation between the temperature range and the charging/discharging duration or UR when the convergence is completed. On the other hand, when operated under temperature range from 40 °C to 73 °C, the charging/discharging duration and UR appears to be convergent faster than operations from 50 °C to 83 °C.

3.4. Influence of switching temperature

Charging and discharging switching temperature, ST_C and ST_D, are two of the most significant parameters for the cyclic operation of single-tank heat storage system in industrial application. Different switching temperatures lead to different completeness of charging and discharging, and hence the variations of convergent temperature distribution, charging/discharging duration and utilization rate. To discuss the influence of the switching temperature, experimental results of different working conditions are presented with ST_C of 57 °C, 65 °C and 73 °C as well as ST_D of 78 °C, 73 °C, 67 °C and 60 °C, as listed in Table 3.

Fig. 7 presents the convergent charging/discharging temperature profiles with different switching temperatures. Fig. 7(a) illustrates that both the charging and discharging convergent temperature profiles are influenced by ST_C in varying degrees. It is obvious that the charging convergent temperature profiles are strongly related to ST_C while the discharging convergent temperature profiles show less difference with different ST_C. With higher ST_C, the charging profiles tend to be flatter.

Shown in Fig. 7(b), the ST_D also has similar effect on the convergent temperature profiles. The ST_D has much stronger impact on the discharging convergent temperature profiles than it does on the charging ones. Also, it can be seen that there is high degree of similarity between convergent charging (discharging) temperature profiles if they share similar ST_C (ST_D). Particularly, the temperature profiles demonstrate higher level of consistency when the charging/discharging is more complete.

The influences of switching temperatures are illustrated in Fig. 8, of which Fig. 8(a) shows the charging/discharging duration and Fig. 8(b) shows the charging/discharging utilization rates after convergence. The charging and discharging durations are determined by both ST_C and ST_D. Either increasing the ST_C or decreasing the ST_D results in longer charging/discharging duration. However, ST_C has stronger impact on the charging duration as ST_D does on the discharging duration.

Similar to the charging/discharging duration shown in Fig. 8(a), the UR in Fig. 8(b) is also influenced by both ST_C and ST_D, i.e., the UR becomes higher if the charging or discharging process is more complete. Due to heat dissipation, the discharging UR of each working condition is slightly smaller than the charging UR. Most importantly, since the paraffin wax has small specific heat and

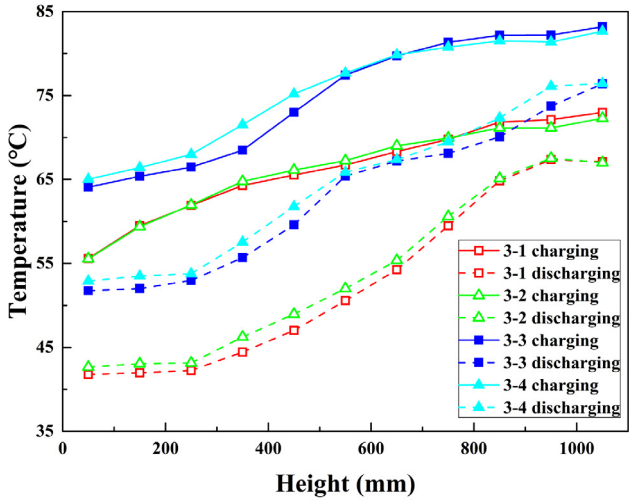

(a) Convergent temperature distribution.

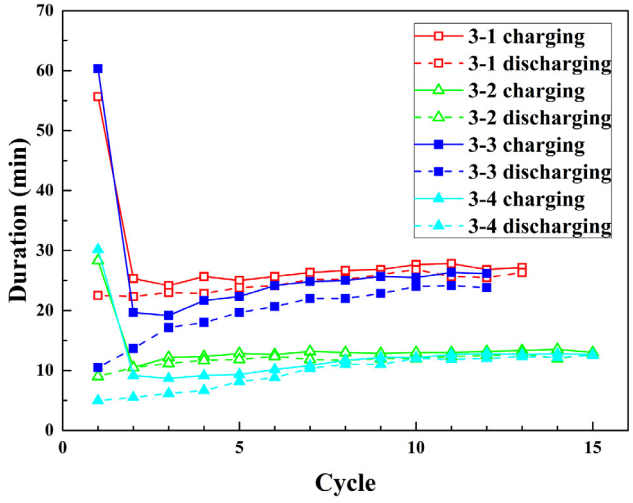

(b) Charging and discharging duration.

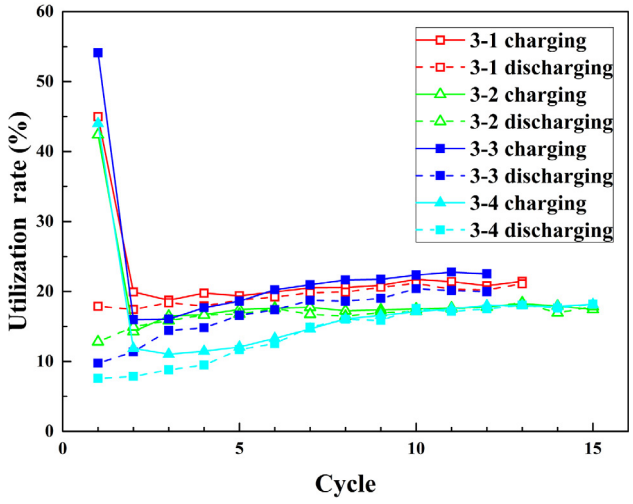

(c) Charging and discharging utilization rate.

Fig. 6. Comparison of cyclic operation with different flow rates and temperature ranges. (a) Convergent temperature distribution; (b) Charging and discharging duration; (c) Charging and discharging utilization rate.

Table 3
Working conditions for the experiments with different switching temperatures.

Case	Q_v (m^3/h)	T_D/T_C (°C)	ST_C/ST_D (°C)	(ST_C^*, ST_D^*)
4-1	0.50	50/83	57/78	(0.21, 0.15)
4-2	0.50	50/83	57/73	(0.21, 0.30)
4-3	0.50	50/83	57/67	(0.21, 0.48)
4-4	0.50	50/83	57/60	(0.21, 0.70)
4-5	0.50	50/83	65/78	(0.45, 0.15)
4-6	0.50	50/83	65/60	(0.45, 0.70)
4-7	0.50	50/83	73/78	(0.70, 0.15)
4-8	0.50	50/83	73/60	(0.70, 0.70)

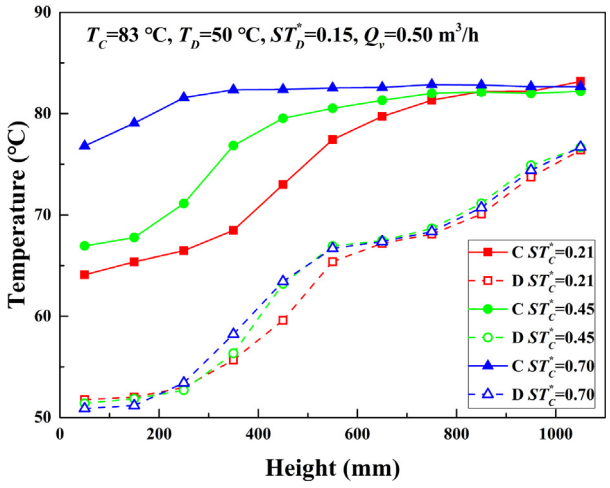

(a) With different charging switching temperature.

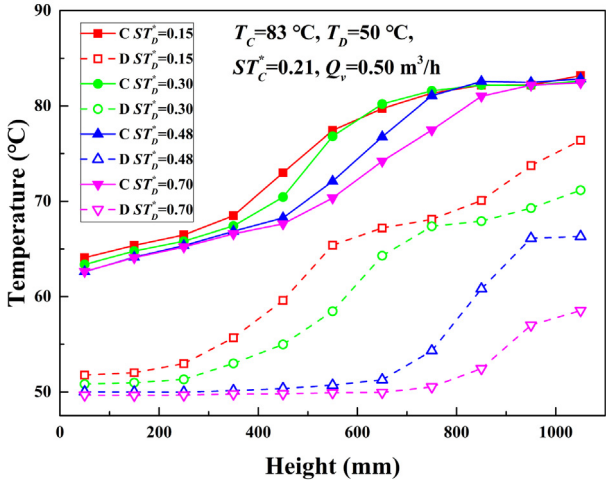

(b) With different discharging switching temperature.

Fig. 7. Convergent charging/discharging temperature profiles. (a) With different charging switching temperature. (b) With different discharging switching temperature.

large latent heat, the selection of switching temperatures has a crucial effect on the UR. With the same ST_D, raising ST_C within the range below the PCT helps little to enhance the charging UR, while it increases significantly by raising ST_C from below to above the PCT. For example, under the condition that ST_D = 78 °C (ST_D^* = 0.15), by raising ST_C from 57 °C to 65 °C, the charging and discharging UR increase by only 4.77% and 4.67%, respectively. However, when ST_C increases from 65 °C to 73 °C, the charging and discharging UR increase by 17.35% and 13.24%, respectively.

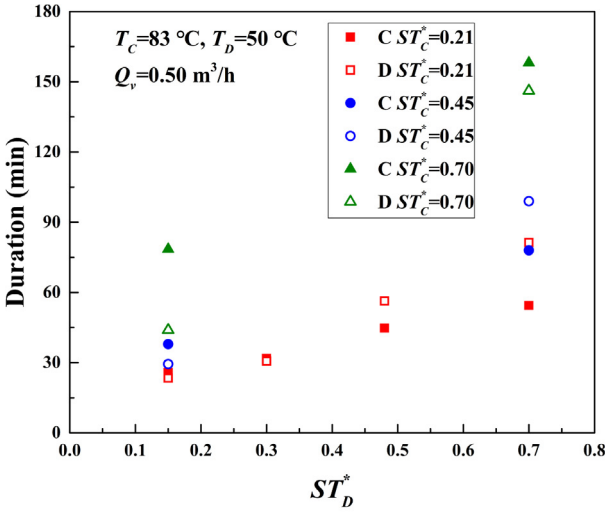

(a) Charging/discharging durations.

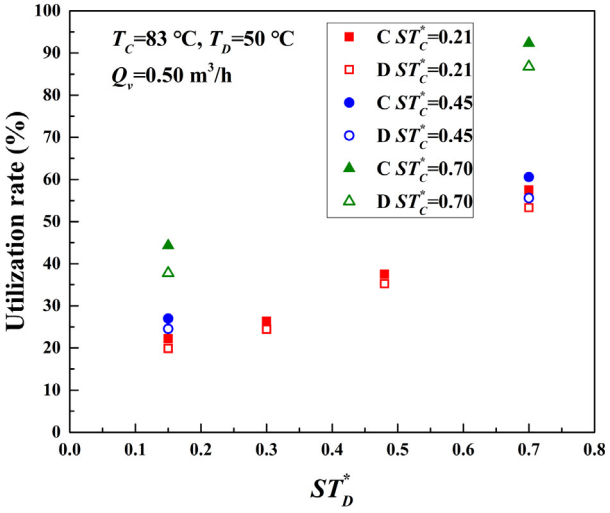

(b) Charging/discharging utilization rates.

Fig. 8. Influences of switching temperatures. (a) Charging/discharging durations. (b) Charging/discharging utilization rates.

Such difference appears to be much more prominent if the discharging is more complete. When ST_D = 60 °C (ST_D^* = 0.70), the charging and discharging utilization rate increase by 3.07% and 2.25% respectively when the ST_C is raised from 57 °C to 65 °C, and by 31.79% and 31.16% respectively when the ST_C is raised from 65 °C to 73 °C.

To illustrate the influence of charging/discharging completeness on the convergence speed of charging/discharging duration and UR, variations of these parameters under the working conditions of 4-1, 4-4, 4-7 and 4-8 listed in Table 3 are presented in Fig. 9 (a) and (b), respectively. In relative term, the four working conditions represent "incomplete charging & incomplete discharging" (IC&ID), "incomplete charging & complete discharging" (IC&CD), "complete charging & incomplete discharging" (CC&ID) and "complete charging & complete discharging" (CC&CD), respectively.

With the exception of IC&ID, each working condition does not demonstrate obvious convergence behavior. Instead, the charging/discharging duration and utilization rate of the other three working conditions become stable soon after the first two cycles. Furthermore, it can also be observed that their axial temperature

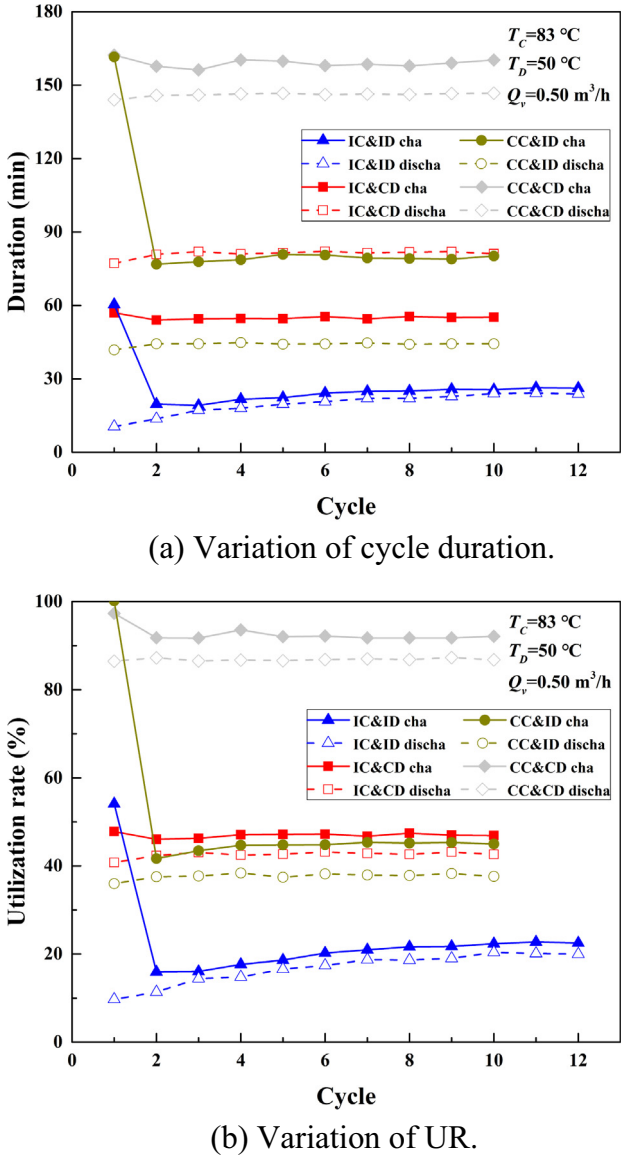

Fig. 9. Influences of charging/discharging completeness. (a) Variation of cycle duration. (b) Variation of UR.

distributions also spend much less cycles to reach convergence than the IC&ID working condition.

During the charging process, the PCM packed bed is heated by the inlet hot water from the top down. In the first charging, the temperature of the top packed bed region rises from 50 °C to over 80 °C after absorbing a large amount of heat from the hot water, which makes the temperature rise of the middle and lower region of the packed bed limited. When turning into discharging process, hot water is extracted from the top along with part of the thermal energy stored within the packed bed. Due to the setting of discharging switching temperature, it is obvious that the thermal energy released during D1 is less than the thermal energy stored during C1 as the tank does not return to the totally discharged status at the end of D1. The top region of the TES tank is able to maintain at high temperature until the discharging is finished. Hence, much less thermal energy is consumed to heat the top packed bed region in the next charging process, leaving more hot water to go through the top region and transfer heat to the PCM packed bed at lower region. With the expansion of hot region inside the tank, more thermal energy can be released during the discharging. That's the reason why the duration and UR appear to be the lowest for D1 and C2 and then gradually climb up. As the cycle number increases, the thermal energy stored into or released from the tank during a single charging or discharging will not increase infinitely as a result of the fixed charging and discharging switching temperature. Instead, both charging and discharging gradually reach stable initial and final states, leading to the convergence behavior of axial temperature distribution, charging/discharging duration and utilization rate of each cycle.

According to the discussions above, the convergence behavior is caused by the difference between the initial statuses of C1 and the following charging processes. As the ST_D decreases, i.e., the completeness of discharging improves, the gap between the initial statuses of each charging becomes narrower. The temperature distribution at the end of C1, charging duration and UR tend to be closer to those of other charging processes, resulting in less cycle number for convergence. As for the working conditions with incomplete discharging, with the increase of ST_C, the initial status for discharging tend to be totally charged. Therefore, each discharging shows similar duration, UR and axial temperature distribution, and hence each charging acts similarly from the second cycle. Consequently, the convergence behavior is more outstanding in the IC&ID working condition. When either charging or discharging get close to complete charging or discharging, less cycles will be spent for the TES tank to reach stability, i.e. the convergence, during the cyclic operation.

As analyzed in Section 3.1, the charging UR and duration of C1 appear to be much higher as a result of the difference of initial statuses between C1 and all other charging processes. Such explanation can be further confirmed in Fig. 9, which shows evidence that the gap between C1 and the rest is narrower under the operations of complete discharging. As the discharging becomes more complete, the end-of-discharging status is closer to totally discharged. Hence, the initial status of the following charging is more similar to that of C1, resulting in closer charging UR and duration.

As discussed above, apart from the heat dissipation, the discharging UR is influenced by the completeness of both charging and discharging. The completeness of charging determines the upper limit of the discharging UR, which is impossible to be larger than the charging UR for the given ST_C and ST_D according to the energy conservation. Meanwhile, the completeness of discharging decides how far will the discharging UR be from its upper limit by influencing the "inherent energy". Specifically, the discharging UR will be equal to the charging UR when it reaches totally discharged status at the end of discharging if the heat dissipation is neglected. The amount of "inherent energy" will be 0 and there will be no difference between the first and the following cycles in this case. Shown in Fig. 9, the discharging UR drops with the decrease of the discharging completeness, leaving more "inherent energy" within the tank. Hence, the difference between the first and the following cycles becomes larger.

4. Conclusions

Experimental study on the water thermocline storage tank with encapsulated paraffin wax packed bed under cyclic operations is presented. The cyclic characteristics are given by discussing the evolutions of temperature distribution, charging/discharging duration and utilization rate under various working conditions. The conclusions are summarized as follows.

(1) As a result of the difference between the initial condition and the end-of-charging/discharging, convergence behavior is observed during the cyclic operation. As the cycle number

increases, the duration and utilization rate of each charging/discharging tend to be stable at a certain value and the temperature distribution tends to be consistent.

(2) The initial status has no significant impact on the TES performance after it reaches convergence, while operations starting with totally charged appear to spend less cycles for convergence than operations starting with totally discharged.

(3) Larger flow rate results in the reduction of utilization rate and the duration of each cycle while it does not affect the convergent speed of these parameters. On the contrary, the influence of working temperature mainly focuses on the convergent speed as lower charging temperature lead to fewer cycles for convergence.

(4) The cyclic operation performance of the water storage tank with PCM packed bed is strongly dependent on the completeness of charging/discharging. Complete charging/discharging is helpful to enhance the utilization rate and reduce the cycle number to reach convergence. Meanwhile, it will also expand the duration for charging/discharging and lead to unstable outlet water temperature during the later period of each charging/discharging.

Declaration of Competing Interest

The authors declared that there is no conflict of interest.

Acknowledgements

The financial supports for this study from the Natural Science Foundation of China (No. 51676069, 51821004) and the National 973 Program of China (No. 2015CB251503) are gratefully acknowledged.

References

[1] H. Wang, W. Yin, E. Abdollahi, R. Lahdelma, W. Jiao, Modelling and optimization of CHP based district heating system with renewable energy production and energy storage, Appl. Energ. 159 (2015) 401–421.
[2] M. Bianchi, A. De Pascale, F. Melino, Performance analysis of an integrated CHP system with thermal and electric energy storage for residential application, Appl. Energ. 112 (2013) 928–938.
[3] S. Hatte, C. Mira-Hernández, S. Advaith, A. Tinaikar, U.K. Chetia, K.V. Manu, K. Chattopadhyay, J.A. Weibel, S.V. Garimella, V. Srinivasan, S. Basu, Short and long-term sensitivity of lab-scale thermocline based thermal storage to flow disturbances, Appl. Therm. Eng. 109 (2016) 936–948.
[4] M.Y. Haller, C.A. Cruickshank, W. Streicher, S.J. Harrison, E. Andersen, S. Furbo, Methods to determine stratification efficiency of thermal energy storage processes – review and theoretical comparison, Sol. Energy 83 (2009) 1847–1860.
[5] X. Ju, C. Xu, G. Wei, X. Du, Y. Yang, A novel hybrid storage system integrating a packed-bed thermocline tank and a two-tank storage system for concentrating solar power (CSP) plants, Appl. Therm. Eng. 92 (2016) 24–31.
[6] E. Oró, A. Castell, J. Chiu, V. Martin, L.F. Cabeza, Stratification analysis in packed bed thermal energy storage systems, Appl. Energ. 109 (2013) 476–487.
[7] G.S. Kumar, D. Nagarajan, L.A. Chidambaram, V. Kumaresan, Y. Ding, R. Velraj, Role of PCM addition on stratification behaviour in a thermal storage tank – an experimental study, Energy 115 (2016) 1168–1178.
[8] A. Felix Regin, S.C. Solanki, J.S. Saini, An analysis of a packed bed latent heat thermal energy storage system using PCM capsules: numerical investigation, Renew. Energ. 34 (7) (2009) 1765–1773.
[9] A.S. Ramana, R. Venkatesh, V.A.A. Raj, R. Velraj, Experimental investigation of the LHS system and comparison of the stratification performance with the SHS system using CFD simulation, Sol. Energy 103 (2014) 378–389.
[10] M. Rady, Granular phase change materials for thermal energy storage: experiments and numerical simulations, Appl. Therm. Eng. 29 (14–15) (2009) 3149–3159.
[11] M. Wu, C. Xu, Y. He, Dynamic thermal performance analysis of a molten-salt packed-bed thermal energy storage system using PCM capsules, Appl. Energ. 121 (2014) 184–195.
[12] K. Cho, S.H. Choi, Thermal characteristics of paraffin in a spherical capsule during freezing and melting processes, Int. J. Heat Mass Tran. 43 (17) (2000) 3183–3196.
[13] L. Xia, P. Zhang, R.Z. Wang, Numerical heat transfer analysis of the packed bed latent heat storage system based on an effective packed bed model, Energy 35 (5) (2010) 2022–2032.
[14] W. Zhao, S. Neti, A. Oztekin, Heat transfer analysis of encapsulated phase change materials, Appl. Therm. Eng. 50 (1) (2013) 143–151.
[15] D.N. Nkwetta, P.E. Vouillamoz, F. Haghighat, M. El-Mankibi, A. Moreau, A. Daoud, Impact of phase change materials types and positioning on hot water tank thermal performance: using measured water demand profile, Appl. Therm. Eng. 67 (2014) 460–468.
[16] K. Kumarasamy, J. An, J. Yang, E.-H. Yang, Novel CFD-based numerical schemes for conduction dominant encapsulated phase change materials (EPCM) with temperature hysteresis for thermal energy storage applications, Energy 132 (2017) 31–40.
[17] Z. Liao, C. Xu, Y. Ren, F. Gao, X. Ju, X. Du, A novel effective thermal conductivity correlation of the PCM melting in spherical PCM encapsulation for the packed bed TES system, Appl. Therm. Eng. 135 (2018) 116–122.
[18] M. Wu, C. Xu, Y. He, Cyclic behaviors of the molten-salt packed-bed thermal storage system filled with cascaded phase change material capsules, Appl. Therm. Eng. 93 (2016) 1061–1073.
[19] Z. Liao, G. Zhao, C. Xu, C. Yang, Y. Jin, X. Ju, X. Du, Efficiency analyses of high temperature thermal energy storage systems of rocks only and rock-PCM capsule combination, Sol. Energy 162 (2018) 153–164.
[20] A. De Garcia, L.F. Cabeza, Numerical simulation of a PCM packed bed system: a review, Renew. Sust. Energ. Rev. 69 (2017) 1055–1063.
[21] K. Nithyanandam, R. Pitchumani, A. Mathur, Analysis of a latent thermocline storage system with encapsulated phase change materials for concentrating solar power, Appl. Energ. 113 (2014) 1446–1460.
[22] K. Nithyanandam, R. Pitchumani, Optimization of an encapsulated phase change material thermal energy storage system, Sol. Energy 107 (2014) 770–788.
[23] A. Bruch, S. Molina, T. Esence, J.F. Fourmigué, R. Couturier, Experimental investigation of cycling behaviour of pilot-scale thermal oil packed-bed thermal storage system, Renew. Energ. 103 (2017) 277–285.
[24] A. Bruch, J.F. Fourmigué, R. Couturier, Experimental and numerical investigation of a pilot-scale thermal oil packed bed thermal storage system for CSP power plant, Sol. Energy 105 (2014) 116–125.
[25] M.-J. Li, Y. Qiu, M.-J. Li, Cyclic thermal performance analysis of a traditional single-layered and of a novel multi-layered packed-bed molten salt thermocline tank, Renew. Energ. 118 (2018) 565–578.
[26] J.D. McTigue, C.N. Markides, A.J. White, Performance response of packed-bed thermal storage to cycle duration perturbations, J. Energy Storage 19 (2018) 379–392.
[27] Z. He, X. Wang, X. Du, M. Amjad, L. Yang, C. Xu, Experiments on comparative performance of water thermocline storage tank with and without encapsulated paraffin wax packed bed, Appl. Therm. Eng. 147 (2019) 188–197.
[28] A. Sharma, V.V. Tyagi, C.R. Chen, D. Buddhi, Review on thermal energy storage with phase change materials and applications, Renew. Sust. Energ. Rev. 13 (2009) 318–345.
[29] S.D. Sharma, H. Kitano, K. Sagara, Phase change materials for low temperature solar thermal applications, Res. Rep. Fac. Eng. Mie Univ. 29 (2004) 31–64.